

# Proceedings of the Institution of Mechanical Engineers, Part H: Journal of Engineering in Medicine

<http://pih.sagepub.com/>

---

## Estimating the density of femoral head trabecular bone from hip fracture patients using computed tomography scan data

Juan F Vivanco, Travis A Burgers, Sylvana García-Rodríguez, Meghan Crookshank, Manuela Kunz, Norma J MacIntyre, Mark M Harrison, J Tim Bryant, Rick W Sellens and Heidi-Lynn Ploeg

*Proceedings of the Institution of Mechanical Engineers, Part H: Journal of Engineering in Medicine* 2014 228: 616

originally published online 19 June 2014

DOI: 10.1177/0954411914540285

The online version of this article can be found at:

<http://pih.sagepub.com/content/228/6/616>

---

Published by:



<http://www.sagepublications.com>

On behalf of:



[Institution of Mechanical Engineers](http://www.imechE.org)

Additional services and information for *Proceedings of the Institution of Mechanical Engineers, Part H: Journal of Engineering in Medicine* can be found at:

**Email Alerts:** <http://pih.sagepub.com/cgi/alerts>

**Subscriptions:** <http://pih.sagepub.com/subscriptions>

**Reprints:** <http://www.sagepub.com/journalsReprints.nav>

**Permissions:** <http://www.sagepub.com/journalsPermissions.nav>

**Citations:** <http://pih.sagepub.com/content/228/6/616.refs.html>

>> [Version of Record](#) - Jun 25, 2014

[OnlineFirst Version of Record](#) - Jun 19, 2014

[What is This?](#)

# Estimating the density of femoral head trabecular bone from hip fracture patients using computed tomography scan data

Proc IMechE Part H:  
J Engineering in Medicine  
2014, Vol. 228(6) 616–626  
© IMechE 2014  
Reprints and permissions:  
sagepub.co.uk/journalsPermissions.nav  
DOI: 10.1177/0954411914540285  
jih.sagepub.com  


Juan F Vivanco<sup>1,2</sup>, Travis A Burgers<sup>3</sup>, Sylvana García-Rodríguez<sup>1</sup>, Meghan Crookshank<sup>4,5</sup>, Manuela Kunz<sup>5</sup>, Norma J MacIntyre<sup>5</sup>, Mark M Harrison<sup>5,6</sup>, J Tim Bryant<sup>4,5</sup>, Rick W Sellens<sup>4,5</sup> and Heidi-Lynn Ploeg<sup>1</sup>

## Abstract

The purpose of this study was to compare computed tomography density ( $\rho_{CT}$ ) obtained using typical clinical computed tomography scan parameters to ash density ( $\rho_{ash}$ ), for the prediction of densities of femoral head trabecular bone from hip fracture patients. An experimental study was conducted to investigate the relationships between  $\rho_{ash}$  and  $\rho_{CT}$  and between each of these densities and  $\rho_{bulk}$  and  $\rho_{dry}$ . Seven human femoral heads from hip fracture patients were computed tomography-scanned ex vivo, and 76 cylindrical trabecular bone specimens were collected. Computed tomography density was computed from computed tomography images by using a calibration Hounsfield units-based equation, whereas  $\rho_{bulk}$ ,  $\rho_{dry}$  and  $\rho_{ash}$  were determined experimentally. A large variation was found in the mean Hounsfield units of the bone cores ( $HU_{core}$ ) with a constant bias from  $\rho_{CT}$  to  $\rho_{ash}$  of 42.5 mg/cm<sup>3</sup>. Computed tomography and ash densities were linearly correlated ( $R^2 = 0.55$ ,  $p < 0.001$ ). It was demonstrated that  $\rho_{ash}$  provided a good estimate of  $\rho_{bulk}$  ( $R^2 = 0.78$ ,  $p < 0.001$ ) and is a strong predictor of  $\rho_{dry}$  ( $R^2 = 0.99$ ,  $p < 0.001$ ). In addition, the  $\rho_{CT}$  was linearly related to  $\rho_{bulk}$  ( $R^2 = 0.43$ ,  $p < 0.001$ ) and  $\rho_{dry}$  ( $R^2 = 0.56$ ,  $p < 0.001$ ). In conclusion, mineral density was an appropriate predictor of  $\rho_{bulk}$  and  $\rho_{dry}$ , and  $\rho_{CT}$  was not a surrogate for  $\rho_{ash}$ . There were linear relationships between  $\rho_{CT}$  and physical densities; however, following the experimental protocols of this study to determine  $\rho_{CT}$ , considerable scatter was present in the  $\rho_{CT}$  relationships.

## Keywords

Computed tomography, femoral head, trabecular bone, bone density, X-ray attenuation

Date received: 4 December 2013; accepted: 16 May 2014

## Introduction

The success of surgical interventions in orthopaedics depends heavily on the quality of the bone in the region of interest.<sup>1–5</sup> Bone quality, which refers to the physical and mechanical properties of the bone, has been estimated clinically through densitometry measurements using dual-energy X-ray absorptiometry (DXA).<sup>6</sup> DXA measures bone mineral content (expressed in grams) and areal bone mineral density (expressed in grams per square centimetre) and is widely used clinically to diagnose osteoporosis in the hip and spine.<sup>7</sup> Despite its widespread clinical use, and the low radiation exposure for patients, the main limitation of DXA is that it is a projected two-dimensional measurement of X-ray attenuation.

<sup>1</sup>Department of Mechanical Engineering, University of Wisconsin–Madison, Madison, WI, USA

<sup>2</sup>Facultad de Ingeniería y Ciencias, Universidad Adolfo Ibáñez, Viña del Mar, Chile

<sup>3</sup>Van Andel Research Institute, Grand Rapids, MI, USA

<sup>4</sup>Department of Mechanical and Materials Engineering, Queen's University, Kingston, ON, Canada

<sup>5</sup>Human Mobility Research Centre, Kingston General Hospital, Queen's University, Kingston, ON, Canada

<sup>6</sup>Department of Surgery, Queen's University, Kingston, ON, Canada

### Corresponding author:

Heidi-Lynn Ploeg, Department of Mechanical Engineering, University of Wisconsin–Madison, 1513 University Avenue, Madison, WI 53706-1572, USA.

Email: ploeg@engr.wisc.edu

Computed tomography (CT) has emerged as a clinical and research tool to evaluate bone quality and as a basis for finite element (FE) analysis of bone. It provides three-dimensional (3D) distributions of X-ray attenuation (Hounsfield units, HUs) allowing not only the analysis of a 3D geometry but also the measurement of volumetric mineral content;<sup>8–12</sup> and thus, the bone mineral density can be estimated using solid calibrated standards of known density. Previous studies have shown that in addition to mineral density, bone quality is affected by the spatial distribution of mineral.<sup>12,13</sup> These characteristics have motivated studies aimed at relating mineral density derived from CT data ( $\rho_{CT}$ ) to other physical and mechanical properties.<sup>11,14–17</sup> Ultimately, the goal is to assess the mechanical properties for fracture risk evaluation,<sup>13,18–21</sup> surgical planning<sup>22</sup> or subject-specific FE modelling.<sup>19–21,23–28</sup> While patient-specific FE models have been used in pre-surgical planning<sup>28</sup> and to assess a clinical condition,<sup>21</sup> patient-specific models are not yet reliable enough to consistently use clinically because of their limited accuracy in modelling the non-homogeneous, anisotropic mechanical properties of bone.<sup>23</sup> These FE models incorporate two independent relationships, one from HU to density and a second from density to modulus of elasticity, to define material properties from CT scans. These two relationships are independent and can each act as a source of error in the FE model.<sup>23</sup>

Several researchers have related HU or  $\rho_{CT}$  directly to elastic modulus or strength,<sup>2,15,16,29–32</sup> while others have analysed the relationship between  $\rho_{CT}$  and bone density for subsequent estimation of mechanical properties.<sup>17,26,33</sup> Lotz et al.<sup>31</sup> determined a linear relationship between  $\rho_{CT}$  and rehydrated apparent density ( $\rho_{app}$ ) of trabecular bone from the human proximal femur ( $R^2 = 0.73$ ), as have other groups for human trabecular bone ( $R^2 = 0.60–0.89$ ).<sup>2,15</sup> In addition, mineral ash density ( $\rho_{ash}$ )<sup>33,34</sup> and dry apparent density ( $\rho_{dry}$ )<sup>33,35</sup> have been considered as effective predictors of bone strength and stiffness and linearly related to  $\rho_{CT}$ .<sup>17,26,36</sup> For example, Schileo et al.<sup>26</sup> found a strong relationship ( $R^2 = 0.937$ ) between mineral density and  $\rho_{CT}$  for trabecular bone. However, many of the reported relationships for predicting density from image data have a wide variation in their coefficients, particularly the predicted  $\rho_{app}$  at 0 CT density (13.2–170 mg/cm<sup>3</sup>), as well as the statistical strength of the relationships ( $R^2 = 0.60–0.99$ ) (Table 1). This variation in the mathematical relationships limits the use of medical image data as a predictor for density and mechanical properties to investigate bone quality. Additionally, most previous studies have been performed on cadaveric bones with no radiographic evidence of bone disease. Therefore, the purpose of this study was to quantify the ability of CT density obtained using typical clinical CT scan parameters to predict the density of femoral head trabecular bone from hip fracture patients.

In this study, four types of densities, including bulk, dry apparent, ash and CT densities, were measured and their empirical relationships were critically examined. The purpose of this study was to compare CT and ash densities for the prediction of dry and bulk densities of bone cores from the human femoral head, explicitly: (1) the relationships between  $\rho_{ash}$  and both  $\rho_{bulk}$  and  $\rho_{dry}$  and (2) the clinically relevant relationship between  $\rho_{CT}$  and both  $\rho_{bulk}$  and  $\rho_{dry}$ . In addition, this study assessed the coefficient of variation (CV) of the mean HUs of the bone cores (HU<sub>core</sub>) as a statistical parameter to represent texture and heterogeneity. CT scan data were assessed in empirical relationships to predict physical properties of human trabecular bone (Table 3 in Appendix 2).

## Methods

### Scan calibration

In a previous study, we validated a method for determining a repeatable scanner-specific density calibration to determine the relationship between HUs and density. Details for this calibration procedure can be found elsewhere.<sup>37</sup> In brief, four hydroxyapatite mineral content standards (phantoms) were imaged in air using a helical multi-slice CT scanner (LightSpeed Plus; General Electric Medical Systems, Milwaukee, WI, USA) with the following parameters: bone reconstruction algorithm, 120 kVp, 250 mA s, 2.5 mm slice thickness, 1.25 mm spacing and 200 mm field of view resulting in a pixel size of  $0.422 \times 0.422$  mm<sup>2</sup>. This is the standard clinical CT scan protocol used for hip fractures at the collaborating hospital, Kingston General Hospital, Kingston, ON, Canada. The mineral contents of the standards were 100, 400, 1000 and 1750 mg/cm<sup>3</sup> (CIRS Inc., Norfolk, VA, USA), encompassing the density range of human long bone.<sup>38,39</sup> The two standards with the lowest mineral content were custom-made (32.4 mm base diameter, 1.5% taper and 80 mm long) and the remaining two were manufactured as plugs (10 mm diameter and 80 mm long) within a water-equivalent material (1000 mg/cm<sup>3</sup>, part 06217; 1750 mg/cm<sup>3</sup>, part 06221).

To measure the mean HU of the standards, the CT data from the four standards were segmented from the images using Mimics (version 11.00; Materialise, Ann Arbor, MI, USA). The segmented regions were edited to close any open internal holes and then the surface voxels were removed from the mask. These edits ensured that the mean HU was measured without any partial volume effects.<sup>37</sup> A repeatability study determined no significant difference in the mean HU when scanned seven times over 19 weeks (inter-class correlation coefficient, ICC(2,1) = 0.9998, 95% lower limit = 0.9993). A linear regression was used to determine the

**Table 1.** Published relationships between physical densities and medical image data from human trabecular bone: the anatomical site, subjects, samples sizes, specimen sizes, CT scan parameters, regression equations and coefficients of determination.

Study	Bone	Equation	R <sup>2</sup>
Hansson (1986) <sup>35</sup>	3 subjects, 78 ± 6.5 yo, 12 vertebrae, n = 231, 10 × 10 × 10 mm, 1000 m <sup>3</sup>	$\rho_{dry} = 1.614\rho_{ash} + 2$	0.988
Mosekilde (1989) <sup>16</sup>	17 m, 13f, 43–95 yo, 60 vertebrae, n = 30, whole vertebral body, 140 kV, 60 mA, 3 s, 2 mm <sup>3</sup>	$\rho_{ash} = 0.4HU + 63$ (L3) $\rho_{ash} = 0.4HU + 88$ (L2)	0.66 0.58
Hvid (1989) <sup>33</sup>	5 m, 5 f, 60–83 yo, 10 p. tibiae, 7.5 dia × 7.5 mm, 331 mm <sup>3</sup> , 120 kVp, 50 mA	$\rho_{ash} = 0.688HU + 61.3$ (n = 215) $\rho_{dry} = 1.20HU + 101$ (n = 215) $\rho_{dry} = 1.81\rho_{ash} - 17.0$ (n = 255)	0.91 0.88 0.97
Ciarelli (1991) <sup>30</sup>	3 m, 1 f, 55–70 yo, 10 bones, n = 723, 8 × 8 × 1–4 mm, 64–256 mm <sup>3</sup> , 130 kV, 100 mA, 4 s, 1–1.5 mm thickness and spacing	$\rho_{app} = 1.14HU + 118.37$ $\rho_{ash}$ versus $\rho_{app}$ $\rho_{ash}$ versus HU	0.821 0.84 0.89
Rho (1995) <sup>32</sup>	7 m, 1 f, 45–68 yo, 8 p. femurs, n = 128, 10 × 10 × 10 mm, 1000 mm <sup>3</sup> , 120 kVp, 150 mA s, 10 mm thickness	$\rho_{app} = 1.067HU + 131$	0.84
McBroom (1985) <sup>15</sup>	8 vertebrae, n = 48, 9.5 dia × 9–13 mm, 0.638–0.921 cm <sup>3</sup> , 5 mm thickness and spacing	$\rho_{app} = 0.983\rho_{CT} + 13.2$	0.89
Esses (1989) <sup>2</sup>	4 m, 4 f, 62–92 yo, 8 p. femurs, n = 49, 9.5 dia × 5 mm, 354 mm <sup>3</sup> , 120 kVp, 5 mm thickness	$\rho_{app} = 1.9\rho_{CT} + 105$	0.60
Lotz (1990) <sup>31</sup>	2 m, 2 f, 25–81 yo, 4 p. femurs, n = 49, 9 dia × 5 mm, 318 mm <sup>3</sup> , 120 kVp, 240 mA s, 0.7 mm pixel	$\rho_{app} = 1.2\rho_{CT} + 170$	0.73
Keyak (1994) <sup>36</sup>	1 m, 1 f, 40–45 yo, 4 p. tibiae, n = 36, 15 × 15 × 15 mm, 3375 mm <sup>3</sup> , 140 kVp, 70 mA, 3 s, 1.5 mm thickness, 1.08 mm pixels	$\rho_{ash} = 0.953\rho_{CT} + 45.7$ $\rho_{dry} = 1.58\rho_{CT} + 80.4$ (derived) $\rho_{app} = 1.71\rho_{CT} + 93.7$ (derived) $\rho_{app} = 1.79\rho_{ash} + 11.9$ $\rho_{dry} = 1.66\rho_{ash} + 4.57$	0.986 – – 0.984 0.922
Kaneko (2004) <sup>17</sup>	1 m, 2 f, 67–88 yo, 4 d. femurs, n = 22, 15 × 15 × 15 mm, 3375 cm <sup>3</sup> , 80 kVp, 280 mA s, 1 mm thickness and spacing, 0.488 mm pixels	$\rho_{ash} = 0.792\rho_{CT} + 79.8, 114 < \rho_{ash} < 311$	0.978
Schileo (2008) <sup>26</sup>	3 subjects, 3 femurs, 4% formalin large: n = 15, 10 dia × 19 mm, 1490 mm <sup>3</sup> small: n = 5, 10 dia × 5 mm, 393 mm <sup>3</sup> , 120 kVp, 160 mA, 0.625 mm spacing and thickness, 0.3125 mm pixels	$\rho_{ash} = 1.02\rho_{CT} + 51.0$ $\rho_{app} = 3.76\rho_{CT} + 188$ (derived) $\rho_{app} = 3.69\rho_{ash} - 0.26$ , large $\rho_{app} = 1.64\rho_{ash} + 0.01$ , small	0.937 – 0.843 0.572
This study	2 m, 5 f, 66–87 yo, 7 p. femurs, n = 76, 10 dia × 5 mm cores, 393 mm <sup>3</sup> , 120 kVp, 250 mA s, 2.5 mm thickness, 1.25 mm spacing, 0.422 mm pixels	$\rho_{ash} = 0.694\rho_{CT} + 111$ $\rho_{dry} = 1.07\rho_{CT} + 147$ $\rho_{bulk} = 0.799\rho_{CT} + 908$ $\rho_{bulk} = 1.19\rho_{ash} + 768.6$ $\rho_{dry} = 1.52\rho_{ash} - 19.6$	0.545 0.562 0.426 0.780 0.993

m: male; f: female; yo: years old; p.: proximal; d.: distal.  
All density values are in milligram per cubic centimetre.

relationship between mean HU and mineral content for each standard.

### Patient recruitment and specimen retrieval

This study was approved by the Queen's University Research Ethics Board. Over the course of 5 months, patients who suffered a low energy subcapital or transcervical femur fracture were scheduled for hip arthroplasty. Seven patients (five females; age range 66–87 years) provided written informed consent to participate in this study. During surgery, the exposed femoral head was notched on the superior surface, excised from the acetabulum using an extraction screw and wrapped in saline-saturated gauze for storage at –40 °C.

### Specimen preparation, scanning and registration

Each femoral head was thawed for 24 h and CT-scanned ex vivo in air along with the standards, using the same clinical scan parameters as were used for the scan calibration. Although it is known that soft tissue surrounding bone affects X-ray attenuation<sup>37</sup>, the femoral heads were scanned in air. To obtain a reasonable HU to CT density calibration, the standards were also scanned in air. The calibration equation from HU to CT density is specific to the parameters of this study including the scanner, scan parameters and the environment in which the objects were scanned. The effects of scanning media were investigated in a previous study, which provided experimental support for the

**Table 2.** Results from the physical properties of human trabecular bone specimens from CT data and measured experimentally.

ID femur	HU <sub>core</sub>	Density (mg/cm <sup>3</sup> )			
		CT	Bulk	Dry	Ash
ALL (n = 74)	260 ± 115	181 ± 82	1061 ± 118	354 ± 132	245 ± 87
ALL F (n = 39)	222 ± 105 <sup>a</sup>	157 ± 73 <sup>a</sup>	1090 ± 99	363 ± 121	252 ± 79
ALL M (n = 35)	303 ± 111 <sup>a</sup>	209 ± 83 <sup>a</sup>	1070 ± 137	377 ± 142	260 ± 93
68 F (n = 5)	231 ± 80 <sup>b,c</sup>	171 ± 58 <sup>b,c</sup>	1017 ± 136 <sup>c</sup>	365 ± 134	253 ± 87
87 F (n = 10)	266 ± 114 <sup>d</sup>	183 ± 83 <sup>d</sup>	1104 ± 109 <sup>d,k</sup>	374 ± 112 <sup>d</sup>	262 ± 75 <sup>d</sup>
86 F (n = 13)	132 ± 45 <sup>b,d,e,f,g,h</sup>	98 ± 33 <sup>b,d,e,f,g,h</sup>	1023 ± 48 <sup>d,g</sup>	246 ± 76 <sup>d,e,f,g</sup>	175 ± 49 <sup>d,e,f,g</sup>
81 F (n = 5)	271 ± 64 <sup>e,i</sup>	185 ± 48 <sup>e,i</sup>	1058 ± 90 <sup>i</sup>	360 ± 83 <sup>e</sup>	242 ± 57 <sup>e,i</sup>
77 F (n = 6)	296 ± 117 <sup>f</sup>	206 ± 85 <sup>f</sup>	1058 ± 134	405 ± 152 <sup>f</sup>	273 ± 100 <sup>f</sup>
79 M (n = 16)	354 ± 106 <sup>c,g,i,j</sup>	247 ± 79 <sup>c,g,i,j</sup>	1168 ± 72 <sup>c,g,i,j</sup>	452 ± 109 <sup>g,j</sup>	312 ± 70 <sup>i,j</sup>
66 M (n = 19)	261 ± 99 <sup>b,h,j</sup>	177 ± 74 <sup>b,h,j</sup>	987 ± 123 <sup>j,k</sup>	314 ± 138 <sup>j</sup>	217 ± 90 <sup>j</sup>

HU: Hounsfield units; CT: computed tomography.

The specimen ID in the left column designates age (number, in years) and gender ('F' or 'M'). 'ALL' indicates the dataset with pooled data. Although there are differences between samples (as designated by superscripts), there are no statistically significant differences in bulk, dry and ash densities between genders ( $p < 0.05$ ).

practice of imaging the calibration standards in the same environment as the target bone.<sup>37</sup>

After the initial ex vivo CT scan, the femoral heads were sectioned perpendicular to the femoral neck under slow, continuous water irrigation using a diamond-coated band saw (EXAKT 311; Norderstedt, Germany). This orientation was identified using the fovea, the angle of the femoral neck fragment and the superior surgical notch. One to three 7-mm thick slices were obtained from each head. Each slice was submerged in cool water and held using a custom-made jig. A diamond-tipped coring bit was used to remove 10-mm-diameter cylindrical cores from each slice. The position of each core within the slice was mapped with respect to the anterior and superior surfaces of the femoral head. The cores were then placed in a custom-made stainless steel clamp and milled (BF400; Präzi Inc., Plymouth, MA, USA) under cool water to a height of 5 mm (1 mm removed from each end) to ensure parallel planes. A total of 86 cores were machined; 10 were excluded due to damage during machining, resulting in 76 cores. From each femur head, 5–19 cylindrical cores were extracted and subsequently tested (Table 2).

To find the X-ray attenuation of cores as located within the femoral head, the CT data from the initial ex vivo CT scan were used to determine the mean of the voxel HUs within a bone core (HU<sub>core</sub>) for each core. After the cores were removed, the slices of the femoral head were re-assembled, and the remaining bone was CT-scanned (LightSpeed 16; General Electric Medical Systems) using the same imaging parameters as the pre-machined, ex vivo scans. Image segmentation was performed using HU-based thresholding, and 3D geometries were generated from the pre- and post-machined scans with the cores removed (Mimics version 11.00; Materialise). A combination of in-house, pair-point and surface matching algorithms was used to align the pre- and post-machined geometries.<sup>40</sup> The latter was

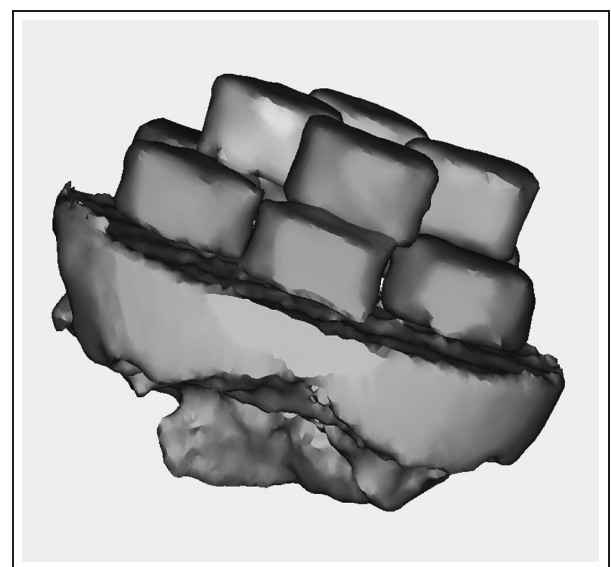


**Figure 1.** The three-dimensional image of one of the femoral head specimens following the subtraction of the post-machining scan from the pre-machining scan. Note that only the cores and the slicing remains result from the subtraction operation. Manual segmentation was required to separate areas between slices where the cores seemed to overlap.

registered to the pre-machined scan using point registration and subtracted from the pre-machined, ex vivo model. The 3D solid of the post-machined head without the cores was subtracted from the 3D solid of the pre-machined head. This resulted in 3D solids of only the cores and the machining remains (Figure 1), thus enabling identification of each core. The number of voxels, HU<sub>core</sub> mean and standard deviation for each core were recorded, excluding boundary voxels to avoid edge artefacts.<sup>26</sup>

To determine the average magnitude of alignment errors between the two CT datasets, pre- and post-machined, the root mean square error between 160 evenly distributed points on the surfaces (pre- and post-

machined) of each femoral head was calculated.<sup>41</sup> A sensitivity analysis was performed on the  $HU_{core}$  of three cores from different femoral head specimens to determine the effect of altering the position of the core by three increments of 1 mm (in each slice) and three increments of 1.25 mm between slices.

### Physical density measurements

To determine the wet bulk volume and bulk densities, the bulk dimensions and wet weight of the cores were measured using vernier calipers (resolution 0.01 mm; Canadian Tire Corporation, Ltd, Toronto, ON, Canada) and an analytical scale (resolution 0.1 mg; Mettler-Toledo, Inc., Columbus, OH, USA). The diameter, height and weight of each core were determined from the mean of three measurements. Hence, bulk density ( $\rho_{bulk}$ ) was calculated by dividing wet mass by bulk volume. Envelopes of folded filter paper were placed in a muffle oven (Blue M Electric, Watertown, WI, USA) at 65 °C for 1 h to dry any excess moisture and then placed in a desiccator (Corning Incorporated, Lowell, MA, USA; desiccant: anhydrous calcium sulphate; W.A. Hammond Drierite Company, Xenia, OH, USA) for 12 min, after which each envelope was weighed. The cores were then secured inside the corresponding envelopes and dried in the oven at 70 °C for 24 h. Enveloped cores were placed in the desiccator for 12 min, immediately after which each core and envelope were weighed. The dried cores were defatted by wrapping the enveloped cores in cheese cloth and placing them in a modified Soxhlet extractor (Corning Incorporated) with ethyl ether for 24 h. After 24 h, the cores were removed from the Soxhlet and left in a fume hood for a further 24 h. The cores were left in the oven at 70 °C for another 24-h period and then placed in the desiccator, as described above, prior to weighing. The dry, defatted bulk dimensions and mass were measured and used to determine the dry apparent density ( $\rho_{dry}$ ) of each cores.

To determine the mineral density ( $\rho_{ash}$ ), the ash weight of the cores was determined. Each core was contained in a pre-weighed crucible and placed in the oven at 100 °C oven for 24 h. Following this initial drying, crucibles with cores were placed in the desiccator for 25 min and then removed and weighed immediately. This step was then repeated for another 24-h period at 100 °C, followed by desiccation and weighing. The crucibles were left in the 700 °C oven for 24 h and then left to cool for 5 h, following which they were placed in a 100 °C oven for 1 h. Once removed from the oven, the crucibles were placed in the desiccator for a period of 25 min and then weighed immediately. This mass, corrected for the mass of the crucible, was divided by dry, defatted bulk volume to calculate  $\rho_{ash}$ .

### Data analysis

All results were expressed as mean  $\pm$  standard deviation and analyses were conducted using the statistics

package Minitab 14 (Minitab Inc., State College, PA, USA). Two methods for obtaining mineral density, namely,  $\rho_{ash}$  and  $\rho_{CT}$ , were compared by using the Bland–Altman (BA) analysis<sup>42</sup> with  $\rho_{ash}$  as the reference measurement. The difference between the two measurements was plotted against the mean of the two measurements. The difference between the means was calculated to represent the bias, and 95% limits of agreement were determined. The Shapiro–Wilk normality test was used to test the assumption of normality of the difference between means.

The empirical relationships between  $\rho_{ash}$  and both  $\rho_{bulk}$  and  $\rho_{dry}$  were analysed with a linear regression model. For each regression, the regression coefficients (slope and intercept) were estimated by the least-squares fit method. Analysis of variance (ANOVA) was performed to test the significance of the valid regression models, whereas the strength of each model was analysed by their coefficient of determination ( $R^2$ ). In all cases, significance level was set at  $p = 0.05$ . For each regression, the standardized residuals were verified as independent normally distributed random variables with 0 mean and constant variance. The significance of slope coefficients with their respective confidence intervals was also reported.

The CV of the  $HU_{core}$  was calculated from the standard deviation over the mean of the voxel HUs within each core. The HUs of each voxel from ex vivo, registered scans were converted to  $\rho_{CT}$  using equation (1). A negative  $\rho_{CT}$  was considered not representative of bone tissue and was therefore set to 0.<sup>43,44</sup> The mean  $\rho_{CT}$  was found for each of the cores and plotted with respect to  $\rho_{bulk}$  and  $\rho_{dry}$ . Linear regressions were performed to determine the predictability of  $\rho_{bulk}$  and  $\rho_{dry}$  from  $\rho_{CT}$  using the same method described above. As a measure of texture and heterogeneity, the  $HU_{core}$  CV was included in a multiple regression model in conjunction with  $\rho_{CT}$  to determine predictors of  $\rho_{dry}$  and  $\rho_{ash}$ .

## Results

The linear regression between HU and mineral content from the standards was found (equation (1)) ( $R^2 = 0.99$ ,  $p < 0.05$ )

$$\rho_{CT} = 0.751 HU - 19.3 \quad (1)$$

where  $\rho_{CT}$  has units of milligram per cubic centimetre.

The root mean square error between points on the surfaces of the registered CT datasets for all the femoral heads ranged from 0.589 to 0.993 mm. The sensitivity analysis performed on the core positioning yielded a change in the  $HU_{core}$  by 0.095%–19.4%, for changes in the position of up to 3.75 mm.

Although the mean  $HU_{core}$  and CT density for the female cores were significantly lower (25%) than the male cores ( $p = 0.002$ ), there were no statistically significant differences between sexes for the bulk ( $p = 0.474$ ), dry ( $p = 0.648$ ) and ash ( $p = 0.693$ ) densities

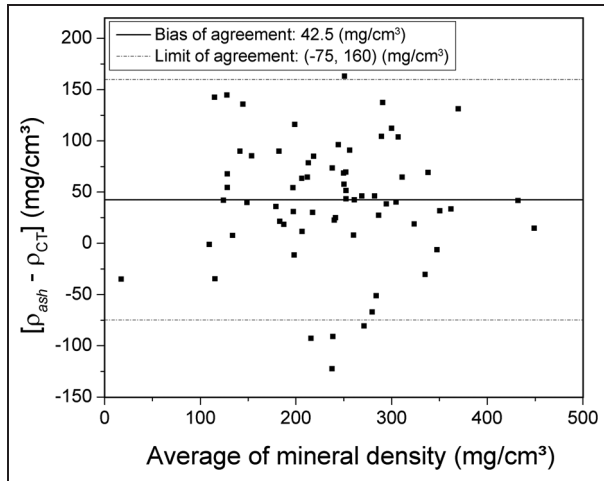


**Figure 2.** Bland–Altman plot for comparing two methods of obtaining mineral density: from ash density ( $\rho_{ash}$ ) and from CT density ( $\rho_{CT}$ ) ( $N = 74$ ).

( $\rho_{bulk}$ ,  $\rho_{dry}$ ,  $\rho_{ash}$ ). A pairwise comparison found that all mean densities of the two male hips were significantly different ( $p = 0.000$ – $0.012$ ) from each other, and the mean densities of the bone cores from the 86-year-old female’s hip were significantly lower ( $p < 0.00001$ ) than the other hips.

Two of the samples had drastically different  $HU_{core}$  CVs than the other samples (CV of 3.41 and  $-12.4$  versus a mean CV of 0.486). These cores also had more than 10% of their voxels with HU less than that of fat (approximately  $-80$ )<sup>44</sup> and therefore were considered as unrepresentative of bone tissue and excluded. Consequently, for the CT density evaluation, only 74 cores were considered. The overall  $HU_{core}$  of 74 cores was 260 ( $\pm 115$ ) with a range of 45–564 (Table 2).

The comparison of  $\rho_{ash}$  and  $\rho_{CT}$  methods to determine mineral density is shown in the BA plot (Figure 2). The difference between methods was constant and consistent as the average  $\rho_{ash}$  increased with a bias of  $42.5 \text{ mg/cm}^3$  across the mean values. This comparison shows that the  $\rho_{CT}$  value falls between 74.9 and  $160 \text{ mg/cm}^3$  for a given  $\rho_{ash}$  (95% confidence interval).

A strong, linear relationship was observed between  $\rho_{ash}$  and  $\rho_{bulk}$  ( $R^2 = 0.78$ ,  $p < 0.05$ ; Figure 3)

$$\rho_{bulk} = 1.19\rho_{ash} + 769 \quad (2)$$

Similarly,  $\rho_{ash}$  was strongly related to  $\rho_{dry}$  ( $R^2 = 0.99$ ,  $p < 0.05$ ; Figure 3)

$$\rho_{dry} = 1.52\rho_{ash} - 19.2 \quad (3)$$

In contrast, the relationships were moderate between  $\rho_{CT}$  and  $\rho_{bulk}$  ( $R^2 = 0.43$ ,  $p < 0.05$ ; Figure 4),  $\rho_{dry}$  ( $R^2 = 0.56$ ,  $p < 0.05$ ; Figure 4) and  $\rho_{ash}$  ( $R^2 = 0.54$ ,  $p < 0.05$ ; Figure 5)

$$\rho_{bulk} = 0.799\rho_{CT} + 909 \quad (4)$$

$$\rho_{dry} = 1.07\rho_{CT} + 147 \quad (5)$$

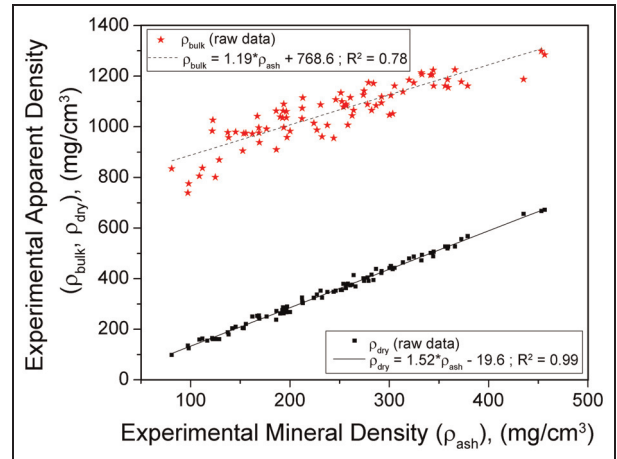


**Figure 3.** Bulk density ( $\rho_{bulk}$ , stars) and dry apparent density ( $\rho_{dry}$ , squares) of all cores plotted with respect to the ash density ( $\rho_{ash}$ ) and fitted with a linear regression, with coefficients of determination of 0.78 and 0.99, respectively.

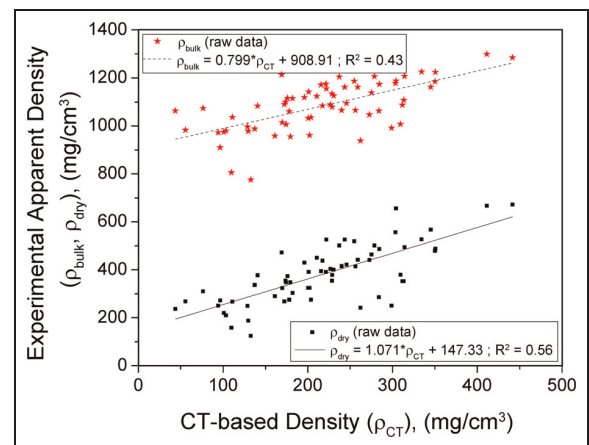


**Figure 4.** Bulk density ( $\rho_{bulk}$ ) and dry apparent density ( $\rho_{dry}$ ) measurements plotted with respect to the CT density ( $\rho_{CT}$ ) calculated from the mean  $HU_{core}$  of each core and fitted with a linear regression. CT: computed tomography.

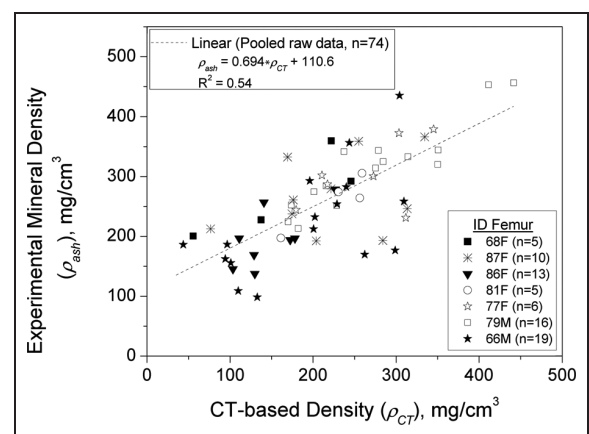


**Figure 5.** Ash density ( $\rho_{ash}$ ) measurements plotted with respect to the CT density ( $\rho_{CT}$ ) calculated from the mean  $HU_{core}$  of each core and fitted with a linear regression. CT: computed tomography.

$$\rho_{ash} = 0.694\rho_{CT} + 111 \quad (6)$$

All density values in equations (2)–(6) are in milligram per cubic centimetre.

## Discussion

This study evaluated the ability of CT data to predict the experimentally measured density of human trabecular bone, focusing on the relationships of  $\rho_{CT}$  versus  $\rho_{bulk}$  and  $\rho_{dry}$ . A bias was found between the mineral density measurement methods. Strong relationships were found between  $\rho_{ash}$  and both  $\rho_{bulk}$  and  $\rho_{dry}$ . On the other hand, correlations of CT density with respect to experimentally measured densities, although statistically significant, only explained between 40% and 60% of the variance. The strongest relationship was found for predicting  $\rho_{dry}$  from  $\rho_{CT}$ .

The BA analysis is a statistical method to present and compare data collected by two different methods<sup>42</sup> to evaluate whether the methods are interchangeable. In this study,  $\rho_{ash}$  was assumed as the reference measurement, and a constant bias of 42.5 mg/cm<sup>3</sup> was found between  $\rho_{ash}$  and  $\rho_{CT}$  such that  $\rho_{ash}$  measures of mineral density exceed  $\rho_{CT}$  measures of mineral density. This result was expected since voxels in the CT data included non-bone material, such as fat. Due to averaging effects, HUs of such voxels were lower and yielded a lower  $\rho_{CT}$ . Limits of agreement show the certainty at the 95% level that  $\rho_{CT}$  values are within 75 mg/cm<sup>3</sup> below and 160 mg/cm<sup>3</sup> above  $\rho_{ash}$ . An underestimation of  $\rho_{CT}$  by 42.5 mg/cm<sup>3</sup> would cause a decrease of 14% in the estimate of  $\rho_{dry}$ , based on equation (5). Using similar linear relationships from previous studies,<sup>2,31</sup> and for example, by Rho et al.,<sup>32</sup> for elastic modulus versus apparent density in the proximal femur (mediolaterally)  $E = 0.01\rho_{app}^{1.86}$ , the estimate of the elastic modulus would have a decrease by 24% with a decrease in  $\rho_{CT}$  of 42.5 mg/cm<sup>3</sup>. Based on this analysis, it was concluded that the two methods for mineral density measurement,  $\rho_{ash}$  and  $\rho_{CT}$ , were not interchangeable. Schileo et al.<sup>26</sup> drew similar conclusions from regression analyses of their data.

The results from this study illustrated that  $\rho_{ash}$  was an excellent predictor of  $\rho_{dry}$ , as has been found in several previous studies.<sup>33,35,36</sup> Several researchers have shown a relationship between  $\rho_{app}$  and elastic modulus;<sup>32,39,45,46</sup> therefore, the prediction of  $\rho_{app}$  from  $\rho_{ash}$  allows for estimation of mechanical properties of bone, useful, for example, in the definition of mechanical properties in bone FE models. However, it has been reported that  $\rho_{dry}$  yields better correlation to mineral density, as specimens for  $\rho_{app}$  are prone to error due to specimen size.<sup>26</sup> Also, Keyak et al.<sup>36</sup> found that there was no significant difference between the use of  $\rho_{dry}$  and  $\rho_{app}$ , with the latter introducing an additional level of experimental complexity and source of error. Taken together, these findings support the measurement of mineral density to estimate  $\rho_{dry}$ .

As expected, the relationship between  $\rho_{ash}$  and  $\rho_{dry}$  ( $R^2 = 0.99$ ) was stronger than the relationship between  $\rho_{ash}$  and  $\rho_{bulk}$  ( $R^2 = 0.78$ ). The  $\rho_{bulk}$  measurements have increased variability due to inclusion of collagen, fat and water in the cores compared to  $\rho_{ash}$  measurements of mineral content only. Similarly, high variability in the data was observed in the relationships between  $\rho_{CT}$  and  $\rho_{bulk}$  and  $\rho_{dry}$ . Again, this was expected due to the trabecular bone's heterogeneity. Moreover, the CT scan resolution was able to capture some of this variation within each core. Correlation equations between CT data and physical density vary greatly among research studies reported in the literature. Table 1 presents several relationships determined between the  $\rho_{bulk}$ ,  $\rho_{app}$ ,  $\rho_{dry}$  or  $\rho_{ash}$  of human trabecular bone samples and HU or  $\rho_{CT}$ ; the corresponding coefficients of determination; the sites of the bone samples; the sizes of the material test specimens and the CT scan parameters. In most studies, voxel HUs were converted into mineral density  $\rho_{CT}$  by a respective calibration curve. This table illustrates the variation in the reported relationships, the slopes ( $m$ ) and particularly the  $y$ -intercepts ( $b$ ), as well as the variation in the correlations ( $R^2$ ) of the relationships. For example, Mosekilde et al.<sup>16</sup> found a good correlation between  $\rho_{ash}$  and the  $HU_{core}$  of cores of trabecular bone from vertebral bodies, concluding that CT data yielded valid predictions of the vertebral trabecular bone mass, as have others for trabecular bone ( $R^2 = 0.58$ – $0.91$ ,  $m = 0.4$ – $0.7$ ,  $b = 61$ – $88$  mg/cm<sup>3</sup>).<sup>16,30,33</sup> Strong correlations between  $\rho_{ash}$  and  $\rho_{CT}$  for human trabecular bone have been found by several research groups ( $R^2 = 0.94$ – $0.99$ ,  $m = 0.79$ – $1.02$ ,  $b = 46$ – $188$ ).<sup>17,26,36</sup> Strong correlations between  $\rho_{app}$  and  $\rho_{CT}$  for trabecular bone have also been reported ( $R^2 = 0.60$ – $0.89$ ,  $m = 0.98$ – $3.7$ ,  $b = 13$ – $188$ ).<sup>2,15,26,31,36</sup> In comparison, the results of this study found similar regression coefficients, but lower correlations for predicting density from  $\rho_{CT}$ . The two unique features of this study that could contribute to the lower  $R^2$  values are as follows: (1) the bone came from hip fracture patients and (2) the CT scan protocol was adopted from the standard protocol used in the clinic. Previous studies have chosen bone and CT scan protocols with the aim of reducing variation; in contrast, this study used bone and scan parameters from the clinic.

Several limitations are acknowledged in this study. The trabecular specimens in this study were retrieved from proximal femurs of elderly, hip fracture patients; therefore, results and conclusions are to be applied to this particular population. It is possible, due to the specific patient group, that the marrow space had a higher fat content, which may have decreased the  $HU_{core}$  and increased its variation. The machining, drying and ashing protocols may have caused errors in the measurements of volumes and weights; however, the high correlations found between the bulk, dry apparent and ash densities (equations (2) and (3)) indicate that the errors in these densities, especially  $\rho_{ash}$  and  $\rho_{dry}$ , were small. The machining of the bone specimens resulted in

loss of bone due to the slicing, coring and milling procedures. The post-machined, re-assembled femoral heads would therefore have lost height (the dimension perpendicular to the plane of the slices) in comparison to their pre-machined geometry. This change in geometry is reflected in the root mean square error (0.589–0.993 mm) between the registration of the pre- and post-machined scans. The effect of the registration error on determining a core's  $HU_{\text{core}}$  was determined (0.095%–19.4%) assuming a worst-case positioning error of 3.75 mm. Each core's  $HU_{\text{core}}$  was determined from the mean HU of all voxels completely within a core (885–5141 voxels per core); however, due to the bone's heterogeneity, the bone cores had large variances associated with their mean  $HU_{\text{cores}}$ . The mean of all the cores CVs was 62%. The main sources of error in the HUs of the voxels were the scan parameters, slice spacing and thickness. These parameters were chosen to mimic clinical scan parameters, not to minimize voxel size partial volume effects. The combination of the inherent variance in the material and sources of error in determining  $HU_{\text{core}}$  would have directly affected  $\rho_{CT}$  (the dependent variable in Figures 4 and 5) and contributed to the low coefficients of determination in equations (4)–(6).

Another potential weakness of  $\rho_{CT}$  is the limitations in defining property–density relationships from in vitro rather than in vivo bones.<sup>20</sup> Due to these limitations in defining physical and mechanical properties from HU, an alternate material mapping strategy has been proposed by Helgason et al.<sup>24</sup> They found decreased error in surface strain predictions when mechanical properties including elastic modulus are distributed within the elements as compared to the conventional method of constant mechanical properties per element.

This study assessed the CV in  $HU_{\text{core}}$  as a statistical parameter to represent texture and heterogeneity of the trabecular cores. This parameter was included in a multiple regression model in conjunction with  $\rho_{CT}$  to determine predictors of  $\rho_{\text{dry}}$  and  $\rho_{\text{ash}}$ . In both cases,  $HU_{\text{core}}$  CV obtained from CT data was not a significant independent predictor of density. Thus, it was concluded that the CT data from the trabecular cores of this study did not convey important structural information for density estimation.

## Conclusion

In conclusion, this study determined a strong linear relationship between the mineral density and bulk and dry apparent densities, concluding that mineral density is an appropriate predictor of both. Through a BA analysis, it was concluded that  $\rho_{CT}$  and  $\rho_{\text{ash}}$  were not adequate surrogates of each other. The relationships between CT density and physical densities were linear; however, due to the limitations of this study, considerable scatter was present. Following the experimental protocol of this study, it was concluded that CT density could not be implemented to accurately predict bulk or

dry densities. Therefore, the limitations of this study, in implementing CT data as a means of estimating bone physical properties, lie in the relationship between the CT data and the mineral density estimate and not in the use of the mineral density to estimate the material properties of trabecular bone.

## Acknowledgements

The authors are grateful to Thomas D. Crenshaw and Debra K. Schneider, UW Department of Animal Sciences, for technical support. Additionally, the authors wish to thank Everett L. Smith for his technical support in bone core preparation.

## Declaration of conflicting interests

The authors declare that there is no conflict of interest.

## Funding

This study received funding from the Canadian Institutes of Health Research (CIHR) NET Grant (QNT-68721), Natural Sciences and Engineering Research Council of Canada and UW Graduate School (S.G.) and also through CIHR Master's Award (M.C.). Funding was also received from DEPUY, a unit of JOHNSON & JOHNSON MEDICAL PRODUCTS, a division of JOHNSON & JOHNSON, INC.

## References

1. Cheal EJ, Hayes WC, White AA 3rd, et al. Stress analysis of compression plate fixation and its effects on long bone remodeling. *J Biomech* 1985; 18: 141–150.
2. Esses SI, Lotz JC and Hayes WC. Biomechanical properties of the proximal femur determined in vitro by single-energy quantitative computed tomography. *J Bone Miner Res* 1989; 4: 715–722.
3. Harrison JW, Howcroft DW, Warner JG, et al. Internal fixation of proximal humeral fractures. *Acta Orthop Belg* 2007; 73: 1–11.
4. Snyder SM and Schneider E. Estimation of mechanical properties of cortical bone by computed tomography. *J Orthop Res* 1991; 9: 422–431.
5. Yoon HG, Heo SJ, Koak JY, et al. Effect of bone quality and implant surgical technique on implant stability quotient (ISQ) value. *J Adv Prosthodont* 2011; 3: 10–15.
6. Wong JCH and Griffiths MR. Precision of bone densitometry measurements: when is change true change and does it vary across bone density values? *Australas Radiol* 2003; 47: 236–239.
7. Blake GM and Fogelman I. The role of DXA bone density scans in the diagnosis and treatment of osteoporosis. *Postgrad Med J* 2007; 83: 509–517.
8. Hoiseth A, Alho A and Husby T. Femoral cortical/cancellous bone related to age. *Acta Radiol* 1990; 31: 626–627.
9. Feldkamp LA, Goldstein SA, Parfitt AM, et al. The direct examination of three-dimensional bone architecture in vitro by computed tomography. *J Bone Miner Res* 1989; 4: 3–11.

10. Jiang Y, Zhao J, Augat P, et al. Trabecular bone mineral and calculated structure of human bone specimens scanned by peripheral quantitative computed tomography: relation to biomechanical properties. *J Bone Miner Res* 1998; 13: 1783–1790.
11. Kowalczyk M, Wall A, Turek T, et al. Computerized tomography evaluation of cortical bone properties in the tibia. *Ortop Traumatol Rehabil* 2007; 9: 187–197.
12. Tabor Z and Rokita E. Quantifying anisotropy of trabecular bone from gray-level images. *Bone* 2007; 40: 966–972.
13. Tanck E, Bakker AD, Kregting S, et al. Predictive value of femoral head heterogeneity for fracture risk. *Bone* 2009; 44: 590–595.
14. Drum MG, Les CM, Park RD, et al. Correlation of quantitative computed tomographic subchondral bone density and ash density in horses. *Bone* 2009; 44: 316–319.
15. McBroom RJ, Hayes WC, Edwards WT, et al. Prediction of vertebral body compressive fracture using quantitative computed tomography. *J Bone Joint Surg Am* 1985; 67: 1206–1214.
16. Mosekilde L, Bentzen SM, Ortoft G, et al. The predictive value of quantitative computed tomography for vertebral body compressive strength and ash density. *Bone* 1989; 10: 465–470.
17. Kaneko TS, Bell JS, Pejcić MR, et al. Mechanical properties, density and quantitative CT scan data of trabecular bone with and without metastases. *J Biomech* 2004; 37: 523–530.
18. MacNeil JA and Boyd SK. Accuracy of high-resolution peripheral quantitative computed tomography for measurement of bone quality. *Med Eng Phys* 2007; 29: 1096–1105.
19. Keyak JH and Falkinstein Y. Comparison of in situ and in vitro CT scan-based finite element model predictions of proximal femoral fracture load. *Med Eng Phys* 2003; 25: 781–787.
20. Schileo E, Taddei F, Malandrino A, et al. Subject-specific finite element models can accurately predict strain levels in long bones. *J Biomech* 2007; 40: 2982–2989.
21. Taddei F, Viceconti M, Manfrini M, et al. Mechanical strength of a femoral reconstruction in paediatric oncology: a finite element study. *Proc IMechE, Part H: J Engineering in Medicine* 2003; 217: 111–119.
22. Moroder P, Resch H, Schnaitmann S, et al. The importance of CT for the pre-operative surgical planning in recurrent anterior shoulder instability. *Arch Orthop Trauma Surg* 2013; 133: 219–226.
23. Poelert S, Valstar E, Weinans H, et al. Patient-specific finite element modeling of bones. *Proc IMechE, Part H: J Engineering in Medicine* 2013; 227: 464–478.
24. Helgason B, Taddei F, Pålsson H, et al. A modified method for assigning material properties to FE models of bones. *Med Eng Phys* 2008; 30: 444–453.
25. Van Rietbergen B. Micro-FE analyses of bone: state of the art. *Adv Exp Med Biol* 2001; 496: 21–30.
26. Schileo E, Dall'ara E, Taddei F, et al. An accurate estimation of bone density improves the accuracy of subject-specific finite element models. *J Biomech* 2008; 41: 2483–2491.
27. Burgers TA, Mason J and Ploeg HL. Initial fixation of a femoral knee component: an in vitro and finite element study. *Int J Exp Comput Biomech* 2009; 1: 23–44.
28. Cattaneo PM, Dalstra M and Frich LH. A three-dimensional finite element model from computed tomography data: a semi-automated method. *Proc IMechE, Part H: J Engineering in Medicine* 2001; 215: 203–212.
29. Duchemin L, Bousson V, Raossanaly C, et al. Prediction of mechanical properties of cortical bone by quantitative computed tomography. *Med Eng Phys* 2008; 30: 321–328.
30. Ciarelli MJ, Goldstein SA, Kuhn JL, et al. Evaluation of orthogonal mechanical properties and density of human trabecular bone from the major metaphyseal regions with materials testing and computed tomography. *J Orthop Res* 1991; 9: 674–682.
31. Lotz JC, Gerhart TN and Hayes WC. Mechanical properties of trabecular bone from the proximal femur: a quantitative CT study. *J Comput Assist Tomogr* 1990; 14: 107–114.
32. Rho JY, Hobatho MC and Ashman RB. Relations of mechanical properties to density and CT numbers in human bone. *Med Eng Phys* 1995; 17: 347–355.
33. Hvid I, Bentzen SM, Linde F, et al. X-ray quantitative computed tomography: the relations to physical properties of proximal tibial trabecular bone specimens. *J Biomech* 1989; 23: 837–844.
34. Hernandez CJ, Beauprè GS, Keller TS, et al. The influence of bone volume fraction and ash fraction on bone strength and modulus. *Bone* 2001; 29: 74–78.
35. Hannson TH, Keller TS and Panjabi MM. A study of the compressive properties of lumbar vertebral trabeculae: effects of tissue characteristics. *Spine* 1986; 11: 56–82.
36. Keyak JH, Lee IY and Skinner HB. Correlations between orthogonal mechanical properties and density of trabecular bone: use of different densitometric measures. *J Biomed Mater Res* 1994; 28: 1329–1336.
37. Crookshank M, Ploeg HP, Ellis R, et al. Repeatable calibration of Hounsfield units to mineral density and effect of scanning medium. *Adv Biomech Appl* 2013; 1: 15–22.
38. Zioupos P, Cook RB and Hutchinson JR. Some basic relationships between density values in cancellous and cortical bone. *J Biomech* 2008; 41: 1961–1968.
39. Carter DR and Hayes WC. The compressive behavior of bone as a two-phase porous structure. *J Bone Joint Surg Am* 1977; 59: 954–962.
40. Ma B and Ellis RE. Robust registration for computer-integrated orthopedic surgery: laboratory validation and clinical experience. *Med Image Anal* 2003; 7: 237–250.
41. Salkind NJ (ed.). *Encyclopedia of research design*. Thousand Oaks, CA: SAGE, 2010.
42. Bland JM and Altman DG. Statistical methods for assessing agreement between two methods of clinical measurement. *Lancet* 1986; 1: 307–310.
43. Perillo-Marcone A, Alonso-Vazquez A and Taylor M. Assessment of the effect of mesh density on the material property discretisation within QCT based FE models: a practical example using the implanted proximal tibia. *Comput Methods Biomech Biomed Engin* 2003; 6: 17–26.
44. Hounsfield GN. Computed medical imaging. *Science (New York, NY)* 1980; 210: 22–28.
45. Helgason B, Perilli E, Schileo E, et al. Mathematical relationships between bone density and mechanical properties: a literature review. *Clin Biomech (Bristol, Avon)* 2008; 23: 135–146.

46. Morgan EF, Bayraktar HH and Keaveny TM. Trabecular bone modulus-density relationships depend on anatomic site. *J Biomech* 2003; 36: 897–904.

$\rho_{ash}$  ash density considered mineral mass over bulk volume  
 $\rho_{bulk}$  bulk density defined as the mass of the intact core, including fat and water, over specimen bulk volume  
 $\rho_{CT}$  computer tomography density derived from Hounsfield units by means of a calibration equation from mineral standards (equation (1))  
 $\rho_{dry}$  dry apparent density considered mass of the intact core excluding fat and water, over specimen bulk volume

**Appendix I**

**Notation**

$b$   $y$ -intercept of regression equation  
 $HU_{core}$  mean of the voxel Hounsfield units within a bone core  
 $m$  slope of regression equation  
 $R^2$  coefficient of determination  
 $\rho_{app}$  wet apparent density considered mass of intact core excluding fat, over bulk volume

**Table 3.** CT scan data, number of voxels, mean, standard deviation and coefficient of variation in HUs and different densities expressed in milligram per cubic centimetre of human trabecular bone specimens.

ID femur	ID core	No. of voxels	$HU_{core}$	Standard deviation HU	Coefficient of variation HU	Density (mg/cm <sup>3</sup> )			
						$\rho_{CT}$	$\rho_{bulk}$	$\rho_{dry}$	$\rho_{ash}$
68 F	213	2311	144	153	1.06	105	801	161	125
	231	1811	154	177	1.15	116	988	338	227
	233	2214	260	262	1.01	195	1156	526	359
	234	2447	327	205	0.626	235	1094	422	292
	235	2026	272	227	0.832	205	1045	376	263
87 F	411	1902	230	132	0.573	156	1006	347	238
	412	1902	329	121	0.368	228	1187	519	359
	413	2059	401	132	0.330	282	1107	352	246
	421	1376	104	122	1.173	71	1073	310	212
	422	1791	232	115	0.497	156	1116	373	261
	423	1862	284	123	0.433	195	1175	391	279
	424	1761	213	111	0.520	143	1214	472	332
	425	2267	349	123	0.352	244	1063	286	193
	426	1614	88	89	1.01	55	869	160	129
86 F	427	1833	425	159	0.374	301	1226	527	366
	511	4250	180	157	0.870	132	1061	275	197
	512	3231	121	117	0.967	83	980	210	145
	521	3047	129	140	1.08	95	996	249	169
	522	3083	148	136	0.922	105	958	179	138
	523	3618	45	95	2.13	33	1027	160	123
	524	3750	131	136	1.04	94	1036	267	196
	525	3623	140	142	1.02	103	1084	377	257
	526	3256	232	179	0.770	171	1089	404	278
	531	4972	149	167	1.12	116	1090	268	194
	532	4740	128	155	1.21	97	984	164	122
	534	5141	125	153	1.22	94	1042	253	167
	535	4170	74	138	1.86	61	974	204	154
81 F	536	4413	116	151	1.30	90	978	188	138
	611	2487	193	102	0.529	127	977	254	169
	613	2891	324	116	0.360	224	1066	414	264
	621	1448	211	110	0.521	140	958	290	197
	622	2688	297	136	0.457	204	1126	401	274
77 F	624	3210	329	125	0.380	228	1162	442	305
	712	3109	377	161	0.428	265	1179	556	373
	713	2462	280	116	0.415	192	1124	446	302
	714	2319	102	107	1.052	66	837	163	112
	722	3817	361	160	0.442	254	1088	352	231
	724	2922	234	136	0.580	158	955	348	244
79 M	726	3112	422	195	0.463	299	1162	568	379
	311	1668	260	118	0.454	177	1142	391	275

(Continued)

Table 3. (Continued)

ID femur	ID core	No. of voxels	HU <sub>core</sub>	Standard deviation HU	Coefficient of variation HU	Density (mg/cm <sup>3</sup> )			
						$\rho_{CT}$	$\rho_{bulk}$	$\rho_{dry}$	$\rho_{ash}$
	312	1952	450	125	0.278	319	1224	488	344
	321	1554	278	101	0.364	189	1171	394	284
	322	1612	465	147	0.317	330	1185	479	320
	323	1601	417	146	0.349	294	1208	494	333
	324	1542	309	104	0.336	212	1205	501	342
	325	1755	377	137	0.365	264	1206	501	343
	326	1520	223	112	0.501	150	1014	324	224
	327	1625	564	187	0.332	404	1285	672	456
	331	1900	374	174	0.466	262	1174	487	325
	332	1781	355	122	0.344	247	1139	464	314
	333	1486	284	145	0.512	195	1090	363	256
	334	1368	227	124	0.549	152	1100	355	252
	335	1448	299	106	0.353	205	1134	355	251
	336	1225	252	145	0.577	171	1115	304	213
	337	1333	524	164	0.313	374	1300	667	453
66 M	811	2394	258	129	0.500	174	905	205	153
	812	3029	310	162	0.522	214	1065	415	282
	821	2270	273	93	0.339	186	1119	430	293
	822	2207	337	98	0.290	234	1162	526	356
	823	2307	287	99	0.384	196	962	325	232
	824	2838	358	117	0.328	249	938	242	169
	825	2168	403	91	0.227	283	992	250	177
	826	1893	146	64	0.441	90	975	220	156
	827	2001	320	124	0.387	221	1080	379	254
	831	2045	287	120	0.418	196	1032	325	212
	832	2029	147	87	0.589	91	973	250	162
	833	885	93	53	0.573	51	1063	237	186
	834	2500	177	84	0.477	113	806	159	109
	835	3000	220	88	0.401	146	739	135	97
	836	3334	190	75	0.396	123	776	125	98
	837	2172	155	81	0.523	97	910	272	187
	838	1942	172	88	0.514	110	1052	437	304
	839	3428	416	182	0.439	293	1008	380	258
	8310	3477	405	127	0.313	285	1188	656	435

HU: Hounsfield units.

The specimen ID in the left column designates age (number, in years) and gender ('F' or 'M').